AIAA JOURNAL
Vol. 34, No. 1, January 1996

Technical Notes

TECHNICAL NOTES are short manuscripts describing new developments or important results of a preliminary nature. These Notes cannot exceed 6 manuscript pages and 3 figures; a page of text may be substituted for a figure and vice versa. After informal review by the editors, they may be published within a few months of the date of receipt. Style requirements are the same as for regular contributions (see inside back cover).

Improvement of Explicit Multistage Schemes for Central Spatial Discretization

Chang-Hsien Tai,* Jiann-Hwa Sheu,† and Pei-Yuan Tzeng‡
Chung Cheng Institute of Technology, Ta-hsi, Tao-yuan, Taiwan 33509, Republic of China

Introduction

THE finite volume explicit flow solver, introduced in Refs. 1 and 2, is still popular for steady-state calculations by solving time-dependent Euler or Navier–Stokes equations. The efficient solver applies some Runge–Kutta time-integration methods that provide fairly good smoothing properties, and it also includes several convergence-acceleration techniques, multigrid relaxation, and efficient dissipation terms. The choice of the multistage parameters, however, is strictly scalar and is carried out by trial and error. There is still some room for improvement of the multistage schemes for suitability of central spatial discretization.

Explicit multistage methods can be designed to provide optimal damping properties for steady-state calculations, based on a given spatial discretization. van Leer et al.[3] developed a minimax procedure for optimally damping the high-frequency errors in a one-dimensional convection equation: putting the zeros of the amplification factor of the multistage scheme on the locus of the Fourier transforms of given spatial discretization. The optimization method was extended to the system of Euler equations by Lynn and van Leer[4] using the local matrix preconditioning of van Leer et al.[5] to make the system more like a scalar equation. The van Leer optimization combined with a modified procedure, suggested by Tai et al.,[6] had been used to design optimally smoothing multistage schemes for upwind-biased spatial discretization, considering the residual smoother with a central differencing operator. These optimal schemes are designed by considering their damping and stability properties only, without regard to time accuracy. In the present study, the multistaging procedure, introduced by Tai et al.,[6] is extended to design optimally smoothing multistage schemes with or without implicit residual smoothing (IRS) and explicit residual smoothing (ERS) for a given central spatial discretization. The damping and stability properties of the designed multistage scheme are investigated and compared. Furthermore, the schemes do effectively enhance the convergence performance of multigrid computations of two-dimensional airfoil flow.

Methodology

To design the optimally smoothing multistage schemes suited for the central spatial discretization, a one-dimensional convection-diffusion equation is considered as the model equation:

$$u_t + u_x + \mu \Delta x^3 u_{xxxx} = 0 \tag{1}$$

where the fourth-order dissipation term is added to prevent instability and it is recalculated in every stage while marching. This model equation is chosen to fit with the use of the effective third-order dissipative term that is implemented throughout smooth region. The multistage schemes designed are considered the artificial viscosity coefficient μ of $\frac{1}{16}$, $\frac{1}{32}$, and $\frac{1}{64}$.

By using the van Leer optimization, the parameters of the optimal schemes for given central differencing, without use of residual smoothing, are shown in Table 1. In the table, ν denotes the Courant–Friedrichs–Lewy (CFL) number, α_k is the kth multistage coefficient, and $|P|_{\max}$ is the equalized minimal maximum of the amplification factor of ℓ-stage scheme in the range $[\pi/2, \pi]$. The contours of the amplification factor of the optimal four-stage scheme for the central spatial differencing with $\mu = \frac{1}{32}$, together with the locus of the Fourier transform $z(\beta)$ of the spatial operator (dashed line) are shown in Fig. 1a. The contour levels for the magnitude of the amplification factor are $|P| = 1, 0.9, 0.8, 0.7, 0.6, 0.5, 0.4, 0.3, 0.2, 0.1, 0.05$, and 0.01. Note that the CFL number achieved in an ℓ-stage scheme is considerably lower than the maximum stable CFL number for that ℓ-stage scheme, which makes the optimal multistage

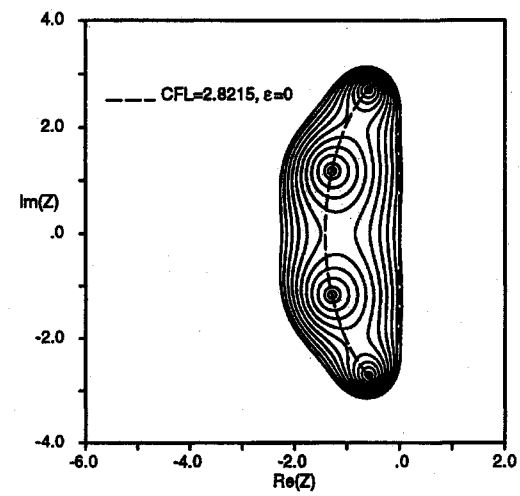

Fig. 1a Locus and contours of optimal four-stage scheme, μ = 1/32.

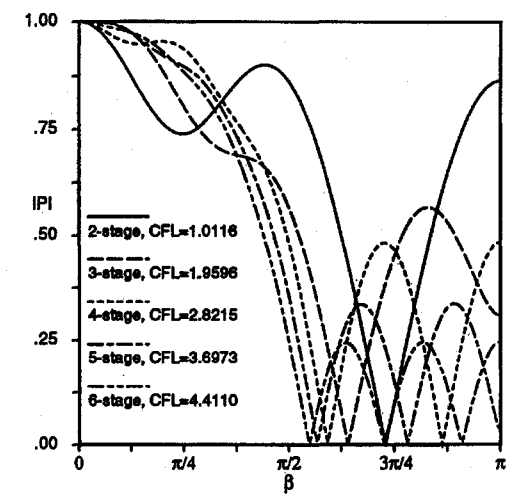

Fig. 1b Amplification factor of optimal multistage schemes, μ = 1/32; without residual smoothing.

Received Jan. 9, 1995; revision received June 16, 1995; accepted for publication July 13, 1995. Copyright © 1995 by the American Institute of Aeronautics and Astronautics, Inc. All rights reserved.

*Professor, Department of Mechanical Engineering.
†Ph.D. Candidate, Department of System Engineering.
‡Associate Professor, Department of Aeronautical Engineering.

Table 1 Optimization multistage parameters for central spatial schemes

	Number of stages				
	2	3	4	5	6
			$\mu = \frac{1}{16}$		
α_1	0.6595	0.2903	0.1635	0.1050	0.0730
α_2	1	0.5252	0.3028	0.1975	0.1388
α_3		1	0.5217	0.3197	0.2179
α_4			1	0.5192	0.3279
α_5				1	0.5163
α_6					1
ν	1.2008	1.8208	2.4376	3.0467	3.6439
$\lvert P\rvert_{max}$	0.7502	0.4587	0.2862	0.1766	0.1095
			$\mu = \frac{1}{32}$		
α_1	1.4330	0.4131	0.2675	0.1617	0.1148
α_2	1	0.5039	0.2732	0.1859	0.1396
α_3		1	0.5898	0.3399	0.2364
α_4			1	0.4944	0.3215
α_5				1	0.5177
α_6					1
ν	1.0116	1.9596	2.8215	3.6973	4.4110
$\lvert P\rvert_{max}$	0.8608	0.5656	0.4611	0.3350	0.2440
			$\mu = \frac{1}{64}$		
α_1	4.2767	0.5601	0.5870	0.2625	0.2135
α_2	1	0.5062	0.2309	0.1601	0.1131
α_3		1	1.0620	0.4280	0.3370
α_4			1	0.4881	0.2928
α_5				1	0.6607
α_6					1
ν	0.6518	1.9311	2.4760	3.7926	4.5769
$\lvert P\rvert_{max}$	0.9506	0.6981	0.7507	0.5280	0.5318

Table 2 CFL number of optimally smoothing multistage scheme for IRS with various smoothing coefficients

	Number of stages				
ε	2	3	4	5	6
			$\mu = \frac{1}{16}$		
0.1	1.4077	2.2685	3.0292	3.7498	4.4743
0.2	1.5167	2.6236	3.6069	4.4673	5.3194
0.3	1.6152	2.8045	3.8591	4.8272	5.8144
0.4	1.7063	2.9697	4.0873	5.1147	6.1646
0.5	1.7914	3.1231	4.2979	5.3974	6.4877
0.6	1.8721	3.2673	4.4950	5.6270	6.7892
0.7	1.9487	3.4037	4.6811	5.8605	7.0738
0.8	2.0220	3.5339	4.8581	6.0825	7.3441
0.9	2.0924	3.6587	5.0272	6.2947	7.6027
1.0	2.1605	3.7785	5.1897	6.4986	7.8508
			$\mu = \frac{1}{32}$		
0.1	1.1509	2.3964	3.4704	4.5601	5.4219
0.2	1.3636	2.7999	3.8958	5.1323	6.1442
0.3	1.4908	3.0802	4.2310	5.5693	6.6669
0.4	1.6074	3.3204	4.5346	5.9630	7.1363
0.5	1.7159	3.5434	4.8145	6.3246	7.5660
0.6	1.8177	3.7525	5.0756	6.6611	7.9658
0.7	1.9141	3.9503	5.3217	6.9777	8.3411
0.8	2.0059	4.1384	5.5553	7.2779	8.6960
0.9	2.0936	4.3184	5.7780	7.5636	9.0345
1.0	2.1779	4.4910	5.9914	7.8373	9.3583
			$\mu = \frac{1}{64}$		
0.1	0.6801	2.2569	2.9466	4.5858	5.4802
0.2	0.8145	2.6874	3.3294	5.1919	6.1269
0.3	0.9473	2.9814	3.6565	5.7032	6.5509
0.4	1.0478	3.2324	3.9549	6.1692	6.8937
0.5	1.1236	3.4650	4.2312	6.6006	7.2307
0.6	1.1947	3.6829	4.4898	7.0044	7.5615
0.7	1.2617	3.8885	4.7339	7.3855	7.8852
0.8	1.3254	4.0838	4.9659	7.7474	8.2016
0.9	1.3861	4.2700	5.1873	8.0929	8.5105
1.0	1.4443	4.4487	5.3996	8.4241	8.8114

Table 3 CFL number of optimally smoothing multistage scheme for ERS with various smoothing coefficients

	Number of stages				
ε	2	3	4	5	6
			$\mu = \frac{1}{16}$		
0.05	1.2359	2.0661	2.7635	3.4400	4.1088
0.10	1.4815	2.4429	3.2197	3.9791	4.7403
0.15	1.4855	2.5716	3.5167	4.4189	5.3160
0.20	1.5516	2.6951	3.6873	4.6369	5.5828
			$\mu = \frac{1}{32}$		
0.05	1.0502	2.2091	3.1812	4.1850	4.9815
0.10	1.2320	2.5700	3.5743	4.7098	5.6372
0.15	1.3500	2.7657	3.8248	5.0372	6.0305
0.20	1.4351	2.9578	4.0663	5.3503	6.4046
			$\mu = \frac{1}{64}$		
0.05	0.6218	2.0689	2.7124	4.2211	5.1113
0.10	0.7233	2.3874	3.0287	4.7218	5.5923
0.15	0.8543	2.6699	3.2802	5.1161	6.0232
0.20	0.9329	2.8786	3.5259	5.5007	6.3076

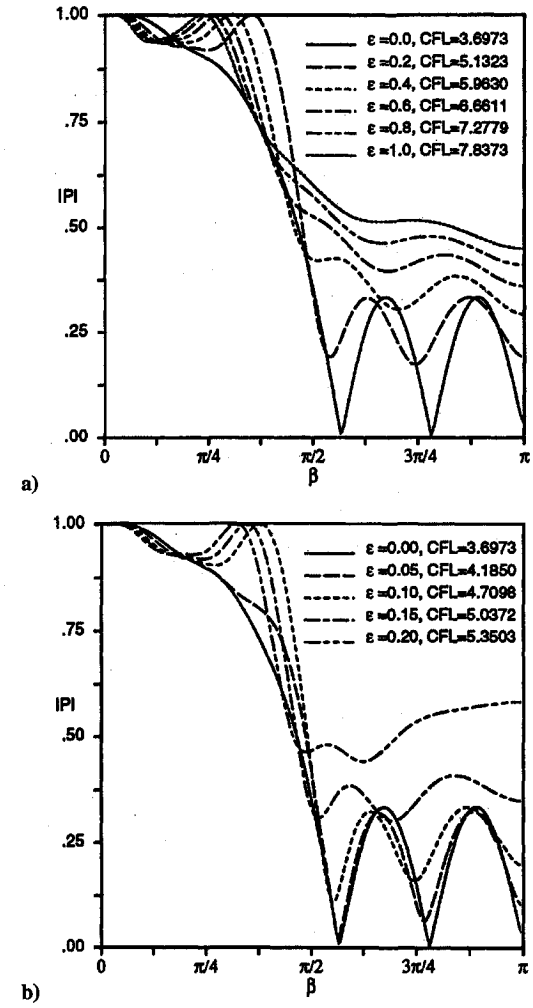

Fig. 2 Amplification factors of the optimal five-stage schemes, $\mu = 1/32$; with different smoothing coefficients with a) IRS and b) ERS.

schemes robust marching schemes. A graphic representation of the amplification factor as a function of the spatial wave number β is given in Fig. 1b for five different multistage schemes, all optimized in the absence of residual smoothing. The good damping properties of the five schemes, especially in high-frequency range, are displayed. It is noted that the amplification factor of the schemes using an odd number of stages cannot reach zero at $\beta = \pi$ to avoid the schemes becoming unstable. When the IRS and ERS, using a second-order central differencing operator,[1,6] are implemented in

every stage of the marching method, the new CFL number for various smoothing coefficients ε are searched by applying the modified procedure and are listed in Tables 2 and 3. Design of schemes with ERS is considered suitable for parallel computing and unstructure grids calculations. It is seen that the CFL number increases with increasing smoothing coefficient. Since there are Fourier modes for ERS, such that the averaged residual could be zero when the old one is not, even for using the modified procedure, the CFL numbers listed in Table 3 are less than 0.25. Figures 2 show that the damping properties become worse with increasing smoothing coefficient.

Application of Optimal Multistage Schemes

A two-dimensional finite volume multigrid Euler solver with central spatial differencing was used to prove the convergence performance of the explicit optimal multistage schemes. In this solver, a third-order dissipative term was added throughout the domain to prevent nonlinear instability, and it was switched into an additional first-order dissipative term to detect shock waves by a pressure-gradient sensor.[1,2] The explicit optimal multistage schemes incorporated with local time stepping were used as the time integrations, and the CFL number obtained from one-dimensional analysis is used to decide the integration time step of two-dimensional calculation by redefining it as in Ref. 4. The residual smoothing is applied only on the finest grid level by using the same coefficient in two different directions in this solver. In addition, the multigrid strategy used in the code is a saw-tooth cycle.[1]

Numerical experiments for the optimal explicit multistage scheme were carried out for the NACA 0012 airfoil in transonic flow at $M_\infty = 0.8$ and 1.25-deg incidence. All testing cases were computed on HP-750 workstations and achieved a drop of residual to 10^{-10}. The computational work units (WU) required for convergence are expressed in term of finest grid residual calculations. A 128×64 O type mesh was generated by an elliptic grid solver. The surface pressure distribution on the airfoil for single- and multigrid calculations are identical and in agreement with the result of Jameson et al.[1]

A Runge–Kutta four-stage scheme, with the maximum allowable CFL number 2.8 and $\mu = \frac{1}{32}$, was chosen to compare with the optimal scheme. Comparisons were implemented both on single- and five-level grids by utilizing the schemes with and without IRS, as shown in Fig. 3. It is seen that the optimal scheme performs better than the Runge–Kutta scheme on different level grids without IRS, presumably because of the better damping properties in the high-frequency range and its slightly larger CFL number. The better convergence of the optimal scheme for five-level calculations may be because of the use of the better damping optimal scheme.

The high-frequency damping of an optimal scheme worsens when the smoothing coefficient ε increases, as shown in Figs. 2. This also can be proved in numerical experiments, as seen in Fig. 4 for IRS. It is seen that the rate of convergence on single-level calculation increases with increasing the residual smoothing coefficient when $\varepsilon \leq 0.6$ as expected, because of the larger CFL number. For the case with $\varepsilon = 0.8$, however, the convergence rate is worse because the

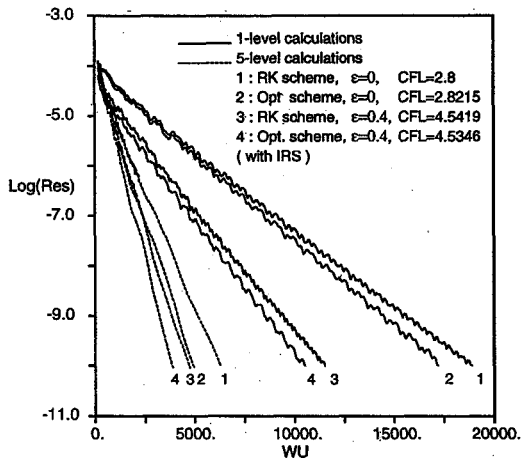

Fig. 3 Comparison of convergence history of optimal and Runge–Kutta four-stage scheme, μ = 1/32.

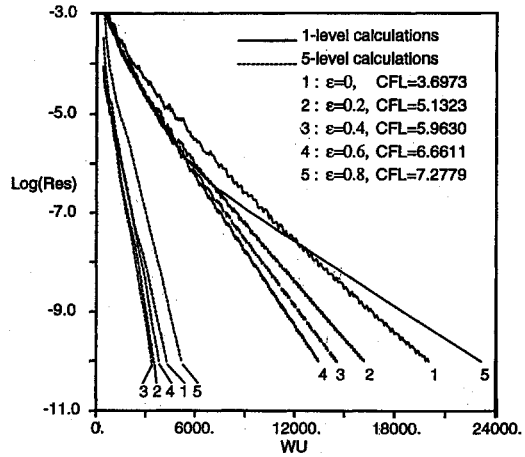

Fig. 4 Convergence history of optimal five-stage schemes, μ = 1/32; with different smoothing coefficients; with IRS.

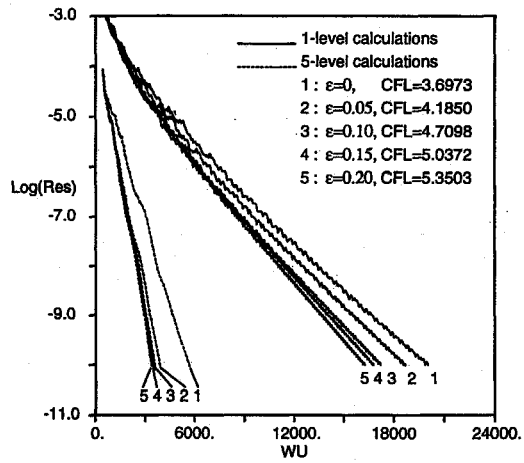

Fig. 5 Convergence history of optimal five-stage schemes, μ = 1/32; with different smoothing coefficients; with ERS.

enlarged CFL number effect cannot overcome the influence of poor damping properties. In our experiments, all of the optimal multistage schemes with $\varepsilon = 0.4$–0.6 are the best choices for using IRS, both in single and multilevel calculations. Figure 5 shows the convergence performance of the optimal five-stage scheme with ERS and the smoothing coefficient from 0 to 0.2 on single- and five-level grids. It is seen that the smoothing coefficient $\varepsilon = 0.2$ yields the best convergence efficiency both in single- and five-level calculations, solely because of its larger CFL number. For ERS, each iteration on single-level grid can save 10% computer time in contrast to that by IRS. Comparing Fig. 4 with Fig. 5, it is seen that the convergence of ERS is faster than that of IRS with the same smoothing coefficient; this is due to the larger CFL number of ERS than that of IRS; however, IRS can use a larger smoothing coefficient. Moreover, it also can be seen that the oscillation in the convergence history become smoother with increasing the smoothing coefficient.

Conclusions

Explicit optimal multistage schemes for second-order space-centered discretization, with and without residual smoothing, have been designed. The damping and stability properties of the multistage schemes have been improved by the optimization procedure. Their applicability in a multigrid code was proved, and the speed up of convergence was caused by the better high-frequency damping. In addition, the optimal scheme with the enlarged CFL number can further enhance the convergence while using the IRS with an appropriately selected smoothing coefficient (0.4–0.6) and using the ERS with smoothing coefficient of 0.2. The optimization procedure can be applied to improve the convergence for the steady-state solver using an explicit Runge–Kutta multistage method for any given spatial discretization.

Acknowledgment

The authors gratefully acknowledge the financial support of the National Science Council of the Republic of China under Grant NSC-82-0401-E-014-009.

References

[1]Jameson, A., Schmidt, W., and Turkel, E., "Numerical Solutions of the Euler Equations by a Finite Volume Method Using Runge–Kutta Time-stepping Schemes," AIAA Paper 81-1259, June 1981.

[2]Jameson, A., "Numerical Solution of the Euler Equations for Compressible Inviscid Fluids," *Numerical Methods for the Euler Equations of Fluid Dynamics*, edited by F. Angrand, A. Dervieux, J. A. Desideri, and R. Glowinski, Society for Industrial and Applied Mathematics, Philadelphia, PA, 1985, pp. 199–245.

[3]van Leer, B., Tai, C.-H., and Powell, K. H., "Design of Optimally Smoothing Multi-stage Scheme for the Euler Equations," AIAA Paper 89-1923, June 1989.

[4]Lynn, J. F., and van Leer, B., "Multi-stage Schemes for the Euler and Navier–Stokes Equations with Optimal Smoothing," AIAA Paper 93-3355, June 1993.

[5]van Leer, B., Lee, W. T., Roe, P. L., Powell, K. G., and Tai, C.-H., "Design of Optimally Smoothing Multistage Scheme for the Euler Equations," *Communications in Applied Numerical Method*, Vol. 8, 1992, pp. 761–769.

[6]Tai, C.-H., Sheu, J.-H., and van Leer, B., "Optimal Multistage Schemes for Euler Equations with Residual Smoothing," *AIAA Journal*, Vol. 33, No. 6, 1995, pp. 1008–1016.

Use of a Wake-Integral Method for Computational Drag Analysis

J. Mark Janus* and Animesh Chatterjee†
Mississippi State University/National Science Foundation Engineering Research Center for Computational Field Simulation, Mississippi State, Mississippi 39762-6176

Introduction

OVER the past few decades the operational requirements of aircraft have placed a premium on high values of aerodynamic efficiency with aircraft having relatively restricted span lengths. Lift-induced drag, for subsonic aircraft, accounts for almost 50% of the total drag of such aircraft under cruise conditions.[1] As a result, much interest exists in the aerospace community to study the causative mechanism involved and to devise new designs to minimize induced drag while maintaining relatively large values for lift coefficient.

Experimentally, the separation of form drag and induced drag involves detailed flowfield measurements, a task both time consuming and costly. Rapid testing of prototypes via numerical flowfield simulation overcomes some of the time and cost constraints linked with experimental techniques, at the same time providing complete flowfield data at no extra cost. The primary issue of interest in this study is the accurate and reliable calculation of induced drag. This interest developed as a consequence of an effort to numerically simulate an experimental investigation designed to study the effect of some innovative configurational arrangements on induced drag.[2] To predict the induced drag for the configurations studied, a wake-integral method was used. Earlier works using a similar approach[3–5] indicate this to be a relatively accurate technique to calculate the lift and induced drag for a finite wing at moderate angles of attack. In this Note, some procedures that were found to be necessary to produce satisfactory induced drag calculations based on this wake-integral approach are discussed.

Analysis

The flow solver used to numerically simulate the flowfields studied herein is based on a finite volume method to solve the three-dimensional Euler equations. Interface fluxes are determined using a high-resolution Riemann scheme.[2,6] The flow solver incorporates characteristic-based concepts, hence characteristic-variable boundary conditions are employed where applicable.

Traditional approaches to lift and drag evaluation for an aerodynamic configuration use either surface force integration or a measurement of the total forces on the system in the wind tunnel. In a numerical simulation using an Euler method, the simplest method toward calculating lift and drag is based on surface pressure integration. Numerical dissipation present in all numerical flow solvers poses quite a problem when considering this approach. The detrimental effects of numerical dissipation is most pronounced at the leading and trailing edges (regions of high gradients) of the body. As a result significant errors can occur, especially in the drag calculations since these regions of tainted pressures are largely oriented in the streamwise direction. The references cited indicate that a wake-integral method appears to be the most accurate method for evaluating induced drag utilizing present computational fluid dynamics (CFD) capabilities. Therefore the approach used here for induced drag and lift determination is the generalized wake-integral method of Wu et al.[3]

Let $\mathcal{V}(t)$ represent a material volume within a fluid mass at time t that completely encloses a body; see Fig. 1. The volume is bounded by planes normal to the freestream velocity both upstream and downstream of the body and by surfaces parallel to $\boldsymbol{V}$ on the sides. Conservation of linear momentum states that the time rate of change of linear momentum of the material volume $\mathcal{V}(t)$ is equal to the resultant force on the volume. Therefore, for the material volume $\mathcal{V}(t)$ bounded by surface $\mathcal{S}(t)$

$$\boldsymbol{F} = \frac{\mathrm{d}}{\mathrm{d}t}\int_{\mathcal{V}(t)} \varrho \boldsymbol{V}\,\mathrm{d}\mathcal{V} \tag{1}$$

For steady flows with no body or viscous forces, the near-field (integral over $\mathcal{S}_9$) and far-field (integral over $\mathcal{S}_{1,2,3,4,5,6}$) expressions for lift are written as

$$L = \int_{\mathcal{S}_9} p\boldsymbol{n}_y\,\mathrm{d}\mathcal{S} = -\int_{\mathcal{S}_{1,2,3,4,5,6}} [p\boldsymbol{n}_y + \varrho v(\boldsymbol{V}\cdot\boldsymbol{n})]\,\mathrm{d}\mathcal{S} \tag{2}$$

and similarly for drag,

$$D = \int_{\mathcal{S}_9} p\boldsymbol{n}_x\,\mathrm{d}\mathcal{S} = -\int_{\mathcal{S}_{1,2,3,4,5,6}} [p\boldsymbol{n}_x + \varrho u(\boldsymbol{V}\cdot\boldsymbol{n})]\,\mathrm{d}\mathcal{S} \tag{3}$$

The near-field expressions are simply surface pressure integration. It is well established that the near-field method of determining the aerodynamic forces on a body works quite well for lift calculations but is tainted by numerical dissipation for drag calculations.

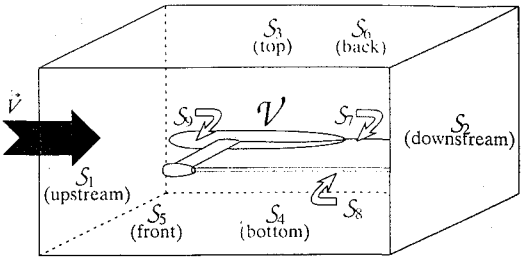

Fig. 1 Control volume for development of the wake-integral theory.

Presented as Paper 95-0535 at the AIAA 33rd Aerospace Sciences Meeting, Reno, NV, Jan. 9–12, 1995; received March 16, 1995; revision received Sept. 5, 1995; accepted for publication Sept. 11, 1995. Copyright © 1995 by the American Institute of Aeronautics and Astronautics, Inc. All rights reserved.

*Assistant Professor, Department of Aerospace Engineering, P.O. Box 6176. Senior Member AIAA.

†Graduate Student, Department of Aerospace Engineering; currently Graduate Student, Syracuse University, 111 College Place, Syracuse, NY 13244-4100.